Anticancer Activity of ST101, A Novel Antagonist of CCAAT/Enhancer Binding Protein β

Emad Darvishi[1], Lila Ghamsari[1], Siok F. Leong[1], Ricardo Ramirez[1], Mark Koester[1], Erin Gallagher[1], Miao Yu[2], Jody M. Mason[2], Gene Merutka[1], Barry J. Kappel[1], and Jim A. Rotolo[1]

ABSTRACT

CCAAT/enhancer binding protein β (C/EBPβ) is a basic leucine zipper (bZIP) family transcription factor, which is upregulated or overactivated in many cancers, resulting in a gene expression profile that drives oncogenesis. C/EBPβ dimerization regulates binding to DNA at the canonical TTGCGCAA motif and subsequent transcriptional activity, suggesting that disruption of dimerization represents a powerful approach to inhibit this previously "undruggable" oncogenic target. Here we describe the mechanism of action and antitumor activity of ST101, a novel and selective peptide antagonist of C/EBPβ that is currently in clinical evaluation in patients with advanced solid tumors. ST101 binds the leucine zipper domain of C/EBPβ, preventing its dimerization and enhancing ubiquitin-proteasome dependent C/EBPβ degradation. ST101 exposure attenuates transcription of C/EBPβ target genes, including a significant decrease in expression of survival, transcription factors, and cell-cycle-related proteins. The result of ST101 exposure is potent, tumor-specific *in vitro* cytotoxic activity in cancer cell lines including glioblastoma, breast, melanoma, prostate, and lung cancer, whereas normal human immune and epithelial cells are not impacted. Further, in mouse xenograft models ST101 exposure results in potent tumor growth inhibition or regression, both as a single agent and in combination studies. These data provide the First Disclosure of ST101, and support continued clinical development of ST101 as a novel strategy for targeting C/EBPβ-dependent cancers.

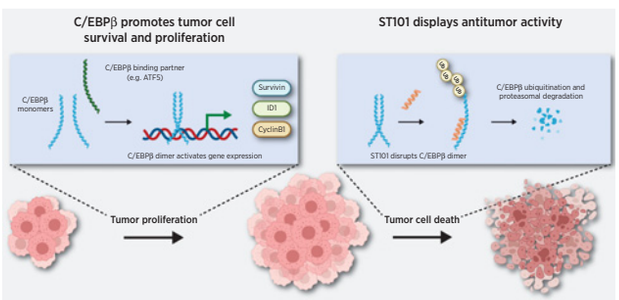

Introduction

CCAAT/enhancer binding protein β (C/EBPβ) is a widely expressed basic leucine zipper (bZIP) transcription factor that regulates genes with functions in organ development (1–3), immune and inflammatory responses such as IL6 expression (4, 5), and macrophage differentiation (6–9). C/EBPβ in differentiated non-myeloid cells is closely regulated and held in a repressed state (10), but may be activated by growth hormone stimulation or PI3K/Akt signaling (11). Overexpression or overactivation of C/EBPβ is observed in cancers including breast, prostate, glioblastoma, melanoma, osteosarcoma, renal cell carcinoma, and colorectal cancer (10; 12–19), contributing to tumor cell proliferation, survival (20), and invasiveness (17, 21). In many of these cancers, enhanced C/EBPβ expression and/or activity inversely correlate with prognosis and survival (10, 14, 22, 23), identifying C/EBPβ as a promising novel therapeutic target.

Transcription factors such as those of the bZIP family have historically been considered "undruggable" due to their lack of enzymatic activity or a defined small-molecule binding site (24, 25). A hallmark of bZIP proteins are C-terminal α-helical leucine zipper domains that mediate interaction-specific homo- and heterodimerization, generating coiled-coil structures that typically stabilize interactions between adjacent basic amino acid-rich DNA-binding domains (26). Dimerization allows for efficient interaction with key consensus DNA sequences as a precursor to regulate gene expression (27, 28). Deletion of the C/EBPβ leucine zipper not only prevents dimerization and DNA binding but results in enhanced C/EBPβ ubiquitination and proteasomal degradation, suggesting that antagonism of dimerization represents a mechanism to negatively regulate their transcriptional activity (29). On the basis of these observations, and the emerging role of C/EBPβ as a driver of diverse cancers, we sought to design a C/EBPβ antagonist peptide as a novel anticancer agent.

Here, we describe the First Disclosure of ST101, a peptide antagonist designed to target the leucine zipper domain of C/EBPβ. ST101 binds to C/EBPβ with nanomolar affinity, effectively disrupting dimerization and DNA binding at consensus binding sites. Exposure to ST101 increased C/EBPβ ubiquitination and proteasome-dependent turnover, resulting in reduced protein levels. Functionally, ST101 induced dose-dependent inhibition of reporter gene activity and C/EBPβ target gene expression. Inhibition of the proteasome rescued C/EBPβ expression and C/EBPβ target gene transcription. Exposure to ST101 increased tumor cell G_0–G_1-phase arrest in U251 glioblastoma and A549 lung adenocarcinoma cells and induced dose-dependent cell death in a panel of tumor cell lines in standard two-dimensional culture conditions and patient-derived breast cancer tumoroids grown in three-dimensional culture. In contrast, ST101 did not significantly impact viability of normal human mammary epithelial cells, peripheral blood mononuclear cells (PBMC) or bone marrow-derived mononuclear cells (BMMC), demonstrating cancer-specific cytotoxicity. Antitumor activity was further demonstrated in

[1]Sapience Therapeutics, Inc., Harrison, New York. [2]Department of Biology & Biochemistry, University of Bath, Claverton Down, Bath, United Kingdom.

Corresponding Author: Jim A. Rotolo, Department of Pharmacology, Sapience Therapeutics, Inc., 500 Mamaroneck Avenue, Harrison, NY 10528. E-mail: jrotolo@sapiencetherapeutics.com

Mol Cancer Ther 2022;21:1632–44

doi: 10.1158/1535-7163.MCT-21-0962

U251 glioblastoma, MCF7 breast adenocarcinoma, A375 melanoma, DU145 prostate, or A549 lung adenocarcinoma subcutaneous xenograft models, where ST101 resulted in significant tumor growth inhibition or regression. These data provide compelling evidence for the potent antitumor activity of the C/EBPβ antagonist peptide, ST101, and support its continued investigation in a phase I to II clinical study in patients with advanced unresectable and metastatic solid tumors (ClinicalTrials.gov ID: NCT04478279).

Materials and Methods

Peptide synthesis

ST101 (*H_2N*-vaeareelerlearlgqargelkkwkmrrnqfwlklqr-*OH*) was synthesized by Fmoc solid-phase peptide synthesis (SPPS) and the mass and sequence were confirmed by mass spectrometry (see Supplementary Materials and Methods and Supplementary Tables S1–S4 for full description). ST101 solution was prepared from lyophilized powder in sterile milli-Q H_2O containing 270 mmol/L trehalose to a stock concentration of 2 mmol/L. Peptides corresponding to the leucine zipper regions of C/EBPβ, C/EBPγ, and ATF5 for circular dichroism (CD) studies (Supplementary Table S5) were synthesized via Fmoc SPPS (30) on a PCAS ChemMatrix Rink amide resin using a Liberty Blue microwave peptide synthesizer (CEM), and blocked at the termini by acetylating the N-terminus and incorporating an amide group at the C-terminus, using acetic anhydride and Rink amide resin, respectively. Analysis of purified final product by RP-HPLC indicated purities >95%.

CD and thermal denaturation experiments

CD was carried out using an Applied Photophysics Chirascan CD apparatus using a 200 μL sample in a CD cell with a 1 mm path length. Samples contained 150 μmol/L total peptide concentration at equimolar concentration for heterodimeric solutions (i.e., 75 μmol/L per peptide) and suspended in 10 mmol/L potassium phosphate and 100 mmol/L potassium fluoride at pH 7.0 prior to analysis. The CD spectra of samples were scanned between 260 and 200 nm in 1 nm steps, averaging 0.5 s at each wavelength. Three scans were averaged at 20°C, 5°C, and once again at 20°C after thermal denaturation to assess helical levels and the ability of the coiled-coil structure to refold. For thermal denaturation experiments, the temperature ramp was set to stepping mode using 1°C increments and paused for 30 seconds at each temperature before measuring ellipticity at 222 nm. For all temperature denaturation experiments, data collection was from 0°C to 80°C. Data points for thermal denaturation profiles represent the averaged signal after 4 seconds of data collection. Melting profiles were ≥95% reversible with equilibrium denaturation curves fitted to a two-state model, derived via modification of the Gibbs–Helmholtz equation (31) to yield the melting temperature (T_m).

C/EBPβ DNA binding activity

Quantitative C/EBPβ binding activity at its consensus DNA binding site was assessed using TransAM C/EBPβ ELISA Kit (Active Motif Inc.). Briefly, 0.3 mg/mL recombinant human C/EBPβ protein was incubated with ST101 for 1 hour and added to a 96-well plate coated with the immobilized oligo 5′-CTTGCGCAATCTATA-3′. After 1 hour of incubation at room temperature, colorimetric quantitation was performed following incubations with C/EBPβ primary antibody and HRP-conjugated secondary antibody, using SpectraMax i3x microplate reader (Molecular Devices) at 450 nm. A negative control peptide containing the scrambled ST101 active domain sequence with an intact penetratin domain (NH2-aegeavraelgraeareqlarekkwkmrrnqfwlklqr-OH; 200 nmol/L) was utilized.

ELISA

Recombinant human C/EBPβ (RayBiotech) was immobilized at a concentration of 3.6 ng/well in 384-well plates (Nunc MaxiSorp, ThermoSci) overnight at 4°C, and wells were blocked for 1 hour at 4°C with 5% bovine serum albumin in TBS. ST101 diluted in TBS was added to the appropriate wells for 1 hour at 4°C, followed by addition of 1 nmol/L recombinant ATF5 for 18 hour at 4°C. Each incubation was followed by three washes with tris-buffered saline (TBS) + 0.1% Tween (TBST). Plate-bound ATF5 was detected by 1 hour incubations at 4°C of 1:1,000 dilution rabbit-anti-ATF5 antibody (ab60126, Abcam) followed by 1:1,000 goat-anti-rabbit IgG-HRP antibody (ab6721, Abcam), with three washes with TBST after each antibody incubation. TMB substrate was added to each well, and absorbance was detected at 450 nm using a SpectraMax M3 plate reader (Molecular Devices). ST101 IC_{50} was calculated by nonlinear regression with four parameters and variable slope using GraphPad Prism 8.3.0 software.

Cell culture and chemicals

Human cell lines A375, A549, DU145, HCT116, MCF7, T98G, and U87 were acquired from ATCC and cultured in MEM (plus 1% MEM NEAA) and McCoy's 5A media (Gibco) supplemented with 1× MycoZap Plus-CL (Lonza Bioscience) and 10% FBS (Gibco) and incubated in 5% CO_2 at 37°C. U251 cells were purchased from Millipore Sigma via European Collection of Authenticated Cell Cultures (ECACC). Two independent vials of U251 from ECACC, referred to as U251 and U251-LS, were identified in viability experiments as having different sensitivity to ST101-induced cell death and maintained as independent cell lines (Supplementary Fig. S1). For all cells, cultures were split every 2 to 3 days and maintained in an exponential growth phase. Mycoplasma testing using MycoAlert PLUS Detection Kit (Lonza Bioscience) was performed every three months on cells in culture. Reporter assay was performed in A549 cells seeded at a density of 2.5×10^4 cells per well of 96-well plates in complete growth medium and incubated overnight at 37°C. Cells were transfected using TransIT-LT1 transfection reagent (Mirus Bio) with 100 ng of C/EBPβ reporter construct (LightSwitch Promoter Reporter vector with a C/EBPβ response element cloned upstream of a basal promoter), or negative control reporter construct that lacks the response element (Active Motif Inc.). After 24 hours, the medium was exchanged with 0.5% FBS medium containing indicated concentrations of ST101. Luminescence was measured following 24 hours exposure to ST101 using LightSwitch Luciferase Reporter Assay reagents (Active Motif Inc.) and a SpectraMax i3x plate reader (Molecular Devices). Statistical significance between groups was determined using Student *t* test. For siRNA experiments, Peli1 (Catalog No. AM16708) and negative control (Catalog No. AM4613) siRNA oligonucleotides were purchased from Thermo Fisher Scientific and 30 pmol siRNA was transfected into U251 cells with Lipofectamine RNAiMAX reagent (Invitrogen, Catalog No. 13778030) according to the manufacturer's protocol. Forty-eight hours posttransfection, cells were treated with 20 μmol/L ST101 for 24 hours, and the total cell lysates were collected for immunoblot analysis.

To evaluate cell cycle, cells were seeded on six-well plates at a density of 1×10^4 per well and cultured overnight for adhesion. Cells were synchronized by double thymidine (2 mmol/L) block procedure, then provided 150 μL of fresh media and 50 μL of ST101 diluted to the appropriate concentration in 270 mmol/L trehalose for 24 hours. Vehicle treated cells served as control. Cells were collected and fixed

with cold 70% ethanol at 4°C overnight. The obtained cells were then washed and resuspended in PBS solution and incubated at 37°C for 30 minutes with 10 mg/mL RNase and 1 mg/mL propidium iodide (PI; BD Biosciences). DNA content analysis was performed by flow cytometry using an Accuri C6 Plus (BD Biosciences), and analysis was performed on BD CSampler Plus software (BD Biosciences). After gating on live cells, single cells were selected via PI width and area signals, and the area histogram for PI was used to determine the percentage of cells in G_1, S, and G_2–M phases.

For viability experiments, cells at a concentration of 5×10^3 to 1×10^4 cells/mL were plated in 96-well tissue culture dishes (Thermo Fisher Scientific) in 100 μL of complete medium and acclimated overnight at 37°C and 5% CO_2. Thereafter, cells were provided 150 μL of fresh media and 50 μL of ST101 diluted to the appropriate concentration in 270 mmol/L trehalose pH 4.5 ± 0.5 for 48 hours. Viability was determined following Annexin V and propidium iodide staining as per manufacturer's instructions (ab14085, Abcam) using the CellInsight CX7 High-Content Screening Platform. Viable cells were represented by the double-negative population. Alternatively, flow cytometry sample acquisition was performed on an Accuri C6 Plus (BD Biosciences), and analysis was performed using BD CSampler Plus software (BD Biosciences).

For patient-derived organoid studies, human breast tumor samples were obtained from adult female patients after written informed consent as part of a non-interventional clinical trial (BTBC study REC no.: 13/LO/1248, IRAS ID 131133). This study had local research ethics committee approval and was conducted adhering to the principles of the Declaration of Helsinki. *Ex vivo* cultures of two dissociated patient-derived breast cancer tumors were set to a cell concentration corresponding to growth of 100 to 300 structures per well in 384-well plates in Ocello PDX media (OcellO B.V.) and hydrogel. ST101 was added to the cultures 24 hours after seeding, and impact on tumoroid viability was performed after 7 days. ST101 impact on tumoroids was quantified following Hoeschst and Rhodamine-Phalloidin staining and imaging as 40 z-sections with a 50 μm step-size and a 4× objective. Z-stack images were processed in OcellO's Ominer image analysis software.

Cycloheximide (Catalog No. C1988) and MG-132 (Catalog No. M7449) were purchased from Sigma-Aldrich. Bortezomib (Catalog No. S1013), TAK-243 (Catalog No. S8341), and MLN4924 (Catalog No. S7109) were obtained from Selleck chemicals.

Immunofluorescence microscopy

U251 cells grown in standard culture were seeded at 10,000 cells/well and incubated overnight at 37°C in 5% CO_2. Cells were exposed to ST101 (0.15–10 μmol/L) at 37°C for 5 or 60 minutes, washed, fixed with 1% paraformaldehyde for 15 minutes, permeabilized with 0.1% Triton-X 100 and ST101 uptake was assessed by CellInsight CX7 High-Content Screening Platform using a 40×/0.60 air objective at room temperature. Immunostaining protocol was as follows: overnight incubation at 4°C with STPX-003 rabbit anti-ST101 polyclonal antibody (1:1,000 dilution), followed by Alexa Fluor 488 conjugated goat anti-rabbit IgG (1:5,000 dilution; ab150077, Abcam) for 45 minutes and 2 μg/mL DAPI for 15 minutes. Cells were individually plotted based upon intensity of the fluorescent signal within the cell nucleus or periphery versus intensity of the nuclear DAPI stain, and gates were established to identify cells positive for ST101 within the nucleus or cytoplasm. Alternatively, 300,000 U251-LS cells in 2 mL of MEM were plated on poly-L-lysine (Sigma) coated cover slips and treated with vehicle or ST101 (20 μmol/L) for 24 hours, fixed in 3.7% formaldehyde for 15 minutes and permeabilized for 10 minutes in 0.25% Triton X-100. Cell were blocked in 1% BSA and stained with anti-C/EBPβ (1:50 dilution; Santa Cruz Biotechnology, Catalog No. sc-7962) overnight followed by Alexa flour 488-conjugated goat anti-mouse (IgG; Thermo Fisher Scientific, Catalog No. A-11001) for 2 hours. Coverslips were mounted in anti-fade reagent (Thermo Fisher Scientific) containing DAPI and imaged. ImageJ (RRID:SCR_003070) was used for quantification of fluorescence intensity.

Western blot assay and antibodies

Cells were plated at a density of 1×10^7 per well of 6-well plate in 2 mL MEM and acclimated overnight at 37°C and 5% CO_2. U251-LS cells were utilized for Western blot experiments unless otherwise indicated. Cells were lysed with RIPA lysis buffer containing trypsin inhibitor for protein extraction and protein concentrations were measured by bicinchoninic acid (BCA) assay. Western blot analysis was performed on cell lysate separated by SDS-PAGE (NuPAGE; 4%–12% Bis-Tris Gels; Thermo Fisher Scientific) and transferred onto a polyvinylidene fluoride membrane. Membranes were blocked with 5% BSA at room temperature for 1 hour prior to immunoblotting. Antibodies against tubulin (ab6046), C/EBPβ (ab32358), C/EBPγ (ab74045), CDK1 (ab133327), Survivin (ab76424, RRID:AB_1524459), and goat Anti-rabbit IgG H&L (Alexa Fluor 488; ab150077) were purchased from Abcam. Antibodies against C/EBPβ (3087S), ID2 (3431S), ID3 (9837S), cyclin A2 (4646T), cyclin B1 (12231T), and c-IAP2 (3130T) were purchased from Cell Signaling Technology. Antibodies against ID1 (sc-133104, RRID:AB_2122863), Peli1 (sc-271065), and β-actin (sc-47778) were purchased from Santa Cruz Biotechnology. Europium-labeled Goat anti-rabbit (R8209) and anti-mouse (R8208) IgG secondary antibodies were obtained from Molecular Devices and detection was performed using SpectraMax i3x imaging system (Molecular Devices). Band intensities were determined using ImageJ (RRID:SCR_003070) and normalized to β-actin, tubulin, or GAPDH as loading control.

For pull-down assays, U251-LS cells (3×10^6) were plated in 10 cm culture dishes overnight and transiently transfected with Myc-tagged C/EBPβ overexpression vector (Origene, Catalog No. RC205882) for 24 hours using TransIT-LT1 transfection reagent (Mirus Bio). pCMV6-AC empty vector (Origene, Catalog No. ps100020) was used as a negative control. Cells were treated with indicated concentrations of ST101 for 24 hours and Myc-tagged C/EBPβ was pulled down from the lysates using Pierce c-Myc-Tag IP/Co-IP Kit (Thermo Fisher Scientific, Catalog No. 23620) according to the manufacturer's instruction. Lysate corresponding to 1 mg of total protein with 10 μL anti-c-Myc agarose beads (5 μg anti-c-myc antibody) was incubated overnight at 4°C. Beads were washed four times with TBS containing 0.05% Tween 20 and samples were boiled in 2× nonreducing sample buffer at 100°C on a heat block for 5 minutes. Elutes were analyzed by immunoblotting using anti-C/EBPβ (Cell Signaling Technology, Catalog No. 3087) and anti-ubiquitin (Cell Signaling Technology, Catalog No. 3933, RRID:AB_2180538) antibodies.

RNA analysis

A549, MCF7, and U251 cells were treated with ST101 for 24 hours. Cell pellets were resuspended in RNAlater (Thermo Fisher Scientific) and total RNA was extracted using Qiagen RNeasy Protect Mini Kit (Quiagen Inc.) according to manufacturer's instructions and treated with Qiagen RNase-free DNase to remove genomic DNA. RNA quality and quantity were measured by Nanodrop, agarose gel electrophoresis, and Agilent 2100 Bioanalyzer. RNA libraries were constructed using NEBNext UltraTM RNA Library Prep Kit. The quality of each library was assessed by Qubit2.0 and insert size was detected by Agilent 2100.

The libraries were sequenced on Illumina HiSeq system with paired end 150. Original image data files from Illumina sequencer were transformed into sequenced reads by CASAVA base recognition (Base Calling), and raw data were stored in FASTQ (fq) files. For qPCR, cDNA was synthesized from total RNA using SuperScript IV VILO Master Mix with ezDNase enzyme (Thermo Fisher Scientific) per manufacturer's protocol. qPCR reactions were set up on a QuantStudio 6 Flex real-time thermal cycler in quadruplicates using 10 ng cDNA, gene-specific primers (0.15 μmol/L each), and Fast SYBR Green Master Mix (Thermo Fisher Scientific). Control reactions without reverse transcriptase were performed. Data were analyzed assuming 100% PCR efficiency. Log2 normalized expression ($2^{-\Delta\Delta Ct}$) and SEM were used to determine fold change of expression in relation to β-actin housekeeping gene and untreated samples (32). Statistical significance between groups was determined using Student *t* test.

Bioinformatic analysis

Low-quality reads containing adaptors, uncertain nucleotides, and *Q* scores of over 50% bases below 5 were filtered out. High-quality raw reads were aligned to the human genome (GRCh38) using STAR aligner (RRID:SCR_004463) and the number of mapped read-pairs were counted based on the GENCODE v36 annotation (GENCODE, RRID:SCR_014966). The data quality control was performed by manually inspecting the density plot, MA plots, PCA plots, correlation heatmap, and PCA association plots, as well as using automatic outlier tests including Euclidean distance, Kolmogorov–Smirnov, Pearson correlation, and Hoeffding *t* test. Gene sets from MSigDB were used for Gene set enrichment analysis (GSEA, RRID:SCR_003199). The MSigDB gene set was compiled of all Hallmark gene sets (H), all oncogenic structure gene sets (C6) and regulatory target gene sets (C3) filtered by the list of terms. GSEA was implemented using the fgsea R package. The statistical significance (nominal *P*-value) of the over-representation was evaluated using a method based on an adaptive multilevel split Monte Carlo scheme. Enrichment scores (ES) were calculated using Kolmogorov–Smirnov-like statistics. FDR-adjusted *P* value was calculated based on Benjamini–Hochberg procedure.

Animals and tumor models

All aspects of animal care were in accordance with the Guide for Care and Use of Laboratory Animals and all experiments were approved by the Institutional IACUC at New York Medical College (NYMC). Female, 6 weeks old, nude Foxn1nu and NOD.CB17-Prkdcscid and C57BL/6 mice obtained from The Jackson Laboratory were housed in a pathogen-free facility at NYMC in sterilized micro-isolator cages and received normal chow and autoclaved hyperchlorinated drinking water (pH 3.0). Cultured cells ($2–5\times10^6$ cells) were washed in PBS and resuspended 1:1 in Matrigel Membrane Matrix HC and RPMI containing 10% FBS prior to inoculation in the mouse flank by SC injection. For the MCF7 ($Her2^{neg}/ER^{pos}/PR^{pos}$) model, mice were supplemented with a 0.5 mg 17β-estradiol 60-day release tablet 1 day prior to tumor inoculation. For the A375 model, tumors were inoculated from cells as described, and serially passaged two times in naïve mice prior to implant of tumor fragments approximately 2 mm^3 into the dorsal flank of recipient mice. To eliminate concern for bias in these experiments, mice were randomized based on tumor size. Mice were treated with vehicle or ST101 at the indicated dose, schedule, and route of administration. Tumor volumes were measured three times per week in nonblinded fashion. Tumor growth inhibition was calculated using the formula $\%TGI = [1 - (\Delta V_t)/(\Delta V_c)]$, where ΔV_c and ΔV_t are the difference in mean volumes from beginning of treatment to end of study for control and treated groups, respectively.

Statistical analysis

All studies were performed at least in triplicate unless otherwise stated. Error bars indicate SEM. Statistical analysis was carried out by GraphPad Prism 7.02 software. Statistical analysis of viability assays was performed using the nonparametric unpaired Mann–Whitney *U* test. The Wilcoxon matched-pairs signed rank test was used for tumor volume data. The two-sided Student *t* test with 95% confidence estimations was used for all other analyses. A value of $P < 0.05$ is considered statistically significant, where all statistically significant values shown in the figures are indicated as: *, $P < 0.05$; **, $P < 0.01$; and ***, $P < 0.005$.

Data and materials availability

RNA sequencing (RNA-seq) data are publicly available at the NCBI Gene Expression Omnibus by GEO accession number: GSE213013. All other data associated with this study are present in the paper or the Supplementary Materials and Methods. Reasonable requests for collaboration involving materials used in the research may be fulfilled provided that a written agreement is executed in advance.

Results

ST101 binds C/EBPβ and disrupts dimerization in solution

As C/EBPβ dimerization is necessary for transcriptional activity, we hypothesized that a novel peptide antagonist designed to bind the C/EBPβ leucine zipper domain and displace endogenous binding partners would function as an onco-repressor of C/EBPβ-mediated gene transactivation. ST101 (*H_2N*-vaeareelerlearlgqar-gelkkwkmrrnqfwlklqr-*OH*) is a linear peptide comprised of D-amino acids, with one region consisting of a leucine zipper optimized to form a coiled-coil interaction with the leucine zipper domain of C/EBPβ, and a second region containing a modified Antennapedia penetratin domain to promote cell and nuclear permeability (33, 34). Analysis of ST101 by CD spectroscopy reveals peaks of 208 and 222 nm, characteristic of a populated α-helical structure (**Fig. 1A**). ST101 generates the same post-melt helical signature following heating to 20°C, indicating refolding after thermal denaturation. Incubation of ST101 with pepsin or trypsin for 16 hours indicate 86.6% and 78.9% stability, respectively, whereas an L-enantiomer analog was completely degraded within 5 minutes (**Fig. 1B**), indicating that ST101 is a proteolytically stable α-helical molecule.

CD spectroscopy was utilized to demonstrate ST101 target engagement with C/EBPβ (leucine zipper domain of C/EBPβ used in CD assays shown in Supplementary Table S5). Equimolar concentrations of ST101 with a peptide containing the bZIP domain of C/EBPβ yielded a significant increase in helical content (**Fig. 1C**, black spectrum) relative to the average of the two individual spectra (**Fig. 1C**, red dashed line). The 222 nm/208 nm ratio for the interaction of ST101 and C/EBPβ bZIP peptide was 1.15, providing evidence for an increase in helical stability compared with the two individual components and evidence for quaternary structure formation. A thermal melt monitoring at 222 nm was performed on the individual peptides as well as the mixture. ST101 displayed an increase in the transition midpoint when in complex with C/EBPβ, indicating that the mixed solution displayed increased thermal stability over the temperature range relative to the mean spectra of the individualized components and suggesting structural stabilization when ST101 interacts with C/EBPβ (**Fig. 1D**). A T_m of 59°C was observed, as determined by least-squares fitting to the denaturation profile, with ST101 displaying an estimated K_D of 175 nmol/L with C/EBPβ, as determined by van't Hoff analysis

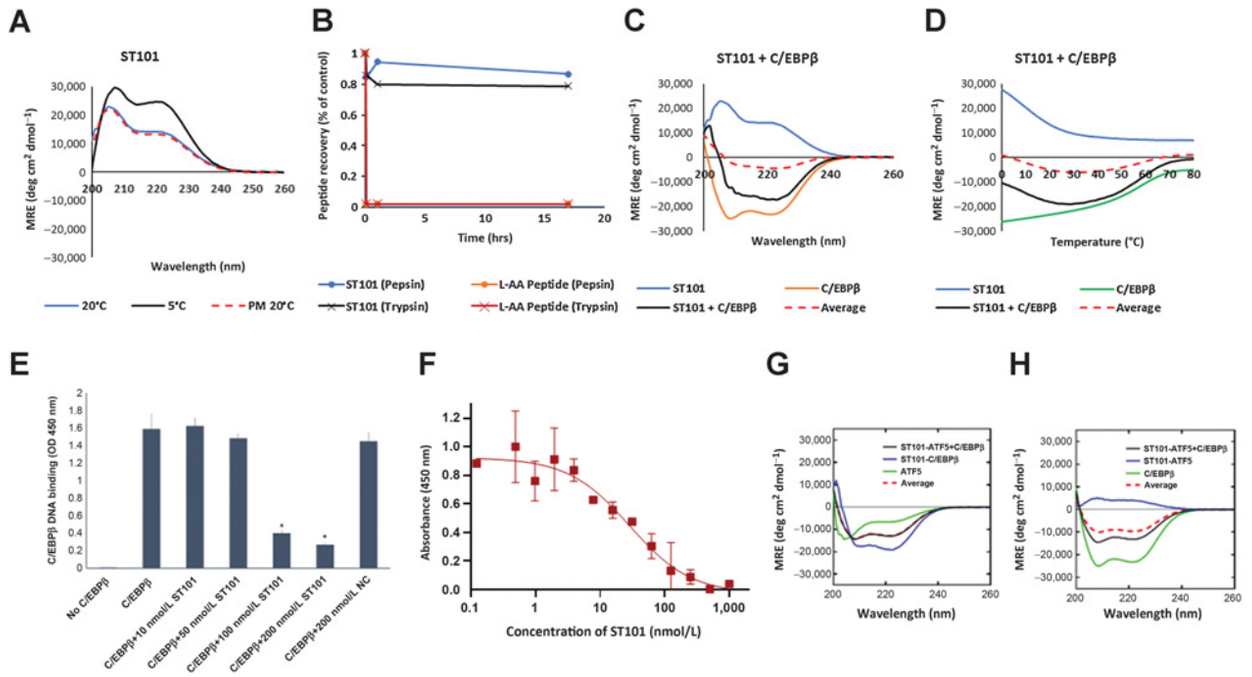

Figure 1.

ST101 binds C/EBPβ and disrupts its dimerization. **A,** CD spectra data of ST101 (150 μmol/L) measured at 20°C, 5°C, or 20°C after cooling to 5°C. Data are presented as mean residue ellipticity (MRE). All experiments were performed in 10 mmol/L potassium phosphate and 100 mmol/L potassium fluoride (pH 7.0). **B,** Stability of ST101 vs. an L-amino acid variant (0.5 mmol/L) following incubation with 0.125% pepsin or trypsin. Peptide stability was measured at 220 nm using HPLC. Data represents mean ± SEM for a minimum of three replicates from two independent experiments for each data point. $P < 0.05$ for ST101 vs. L-aa with both pepsin and trypsin. **C,** CD spectra data for the interaction of ST101 with C/EBPβ. **D,** The thermal stability of peptide pairs measured demonstrated using temperature dependence of the CD signal at 222 nm. Profiles of C/EBPβ and ST101 homodimeric peptides and heterodimers were taken with 1°C increments and tracking the 222 nm signal. Melting profiles for heterodimers are clearly distinct from averages of constituent homodimeric melts, with the cooperative nature of the heterodimeric melting profiles suggesting an apparent two-state process (31). All data were fitted to the two-state model. **E,** C/EBPβ DNA binding ± ST101 or negative control peptide (scrambled ST101 sequence with intact penetratin), as measured by TransAM C/EBPβ ELISA Kit (Active Motif Inc.), following the manufacturer's instructions (*, $P < 0.05$ vs. C/EBPβ alone). **F,** ELISA detection of ST101-mediated disruption of the interaction of plate-bound C/EBPβ with ATF5 indicates and IC_{50} of 24.6 ± 0.9 nmol/L. **G,** CD spectra of dimer exchange experiment in which ATF5 was added to a solution of ST101 and C/EBPβ. **H,** CD spectra of dimer exchange experiment in which C/EBPβ was added to a solution of ST101 and ATF5.

following extraction from thermal denaturation curves and assuming constant ΔH (35).

To evaluate binding specificity, experiments were performed investigating ST101 interactions with the leucine zipper domains of C/EBPγ and ATF5 (Supplementary Table S5). ST101 association with the leucine zipper of C/EBPγ resulted in a complex with increased helical stability compared with the individual components and evidence for quaternary structure formation, however the T_m of the interaction was 37°C, with an estimated K_D of 555 μmol/L, indicating >3,000-fold weaker interaction with C/EBPγ than with C/EBPβ (Supplementary Figs. S2A and S2B). No change in the CD spectrum relative to the average of the individual spectra was observed following analysis of ST101 with leucine zipper of ATF5, indicating no stabilizing interaction between these peptides (Supplementary Figs. S2C and S2D, red dash theoretical average superimposes with the black observed spectrum). Overall, these data suggest that ST101 specifically interacts with the leucine zipper region of C/EBPβ.

Dimerization regulates DNA binding of bZIP transcription factors including C/EBPβ (9, 36). ST101 at an exposure of 200 nmol/L results in 84% reduction of C/EBPβ binding to an immobilized oligonucleotide containing the C/EBPβ consensus binding site (5′-GCAAT-3′), compared with untreated control (**Fig. 1E**). A negative control peptide containing the cell penetrating domain of ST101 with a random α-helical bZIP domain did not impact C/EBPβ binding. These data demonstrate that ST101 disruption of C/EBPβ homodimerization antagonizes DNA binding.

To evaluate the impact of ST101 on C/EBPβ heterodimerization, a competitive ELISA evaluating the association of ATF5 to plate-bound C/EBPβ was used. Addition of ST101 to a constant concentration of 1 nmol/L ATF5 (K_d for C/EBPB-ATF5 PPI = 1.0 nmol/L; Supplementary Fig. S3) resulted in a dose-dependent decrease in ATF5 immunodetection (**Fig. 1F**), with an IC_{50} for ST101 inhibition of ATF5 association with C/EBPβ of 24.6 ± 0.9 nmol/L. Dimer exchange experiments performed by CD spectroscopy confirmed these results. In these experiments, addition of the ATF5 leucine zipper to a premixed solution of ST101 and C/EBPβ did not result in a change in molar ellipticity relative to that of the theoretical summed signals (**Fig. 1G**), suggesting that ATF5 did not disrupt the ST101 and C/EBPβ dimer. In contrast, addition of C/EBPβ leucine zipper to a premixed solution of ST101 and ATF5 resulted in a significant change in ellipticity relative to the average of the component signals (**Fig 1H**, black vs. red dash). The resultant spectrum superimposed the spectra generated by a solution of ST101 with C/EBPβ (Supplementary Fig. S4), suggesting that the same species became populated in both instances. These data indicate that ST101 disrupts C/EBPβ heterodimerization.

ST101 rapidly enters cells and antagonizes C/EBPβ

ST101 contains a modified penetratin domain to enable cellular uptake. To confirm ST101 cellular penetration, scanning immunofluorescence microscopy was performed on U251-LS glioblastma cells exposed to 0.15 to 20 μmol/L ST101 for 5 minutes. Immunostaining was performed using a polyclonal antibody generated against the leucine zipper domain of ST101 and counterstained with DAPI (representative images in **Fig. 2A**) prior to imaging. Data indicates uptake of the peptide into 100% of cells at peptide concentrations of 0.3 μmol/L or greater, with signal reaching saturation at 10 μmol/L. Detection within the nuclear compartment indicates that peak signal was achieved at a concentration of 1.25 μmol/L. Similar results were obtained after 1 hour incubation with ST101.

To examine the functional consequence of C/EBPβ antagonism, the impact of ST101 on C/EBP reporter activity was evaluated. A549 lung carcinoma cells were transiently transfected with a plasmid containing the Renilla luciferase gene with a C/EBP response element cloned upstream of a basal promoter, or a negative control vector that contains a random sequence instead of the C/EBP response element. ST101 resulted in dose-dependent and statistically significant decrease in C/EBP reporter luciferase signal (**Fig. 2B**, $P < 0.05$ for 5 μmol/L and $P < 0.01$ for 40 μmol/L), indicating antagonism of C/EBPβ-mediated gene transactivation. In contrast, ST101 had no impact on luciferase reporter systems containing a random response element or one that carries the promoter of the C/EBPβ gene (Supplementary Fig. S5).

ST101 induces targeted degradation of C/EBPβ

Dimerization provides structural stability to C/EBPβ and protects the protein from degradation by the proteosome (29). To evaluate the impact of ST101 on C/EBPβ protein expression, immunofluorescence microscopy and Western blot analysis were performed. U251-LS cells treated with 20 μmol/L ST101 for 24 hours demonstrated a 34 ± 6% decrease in C/EBPβ expression (**Fig. 2C**; $P = 0.006$ vs. untreated controls). Western blot analysis of total cell extracts from ST101 treated cells confirmed a dose-dependent and statistically significant reduction in C/EBPβ protein levels in U251-LS and HCT116 cell lines 24 hours posttreatment (**Fig. 2D**; Supplementary Fig. S6A), with 20 μmol/L ST101 resulting in 44 ± 1% ($P = 0.0005$) and 40 ± 0.4% ($P = 0.006$) reduction in C/EBPβ protein expression in U251-LS and HCT116 cell lines, respectively. Similar results were observed in U251 cells at ST101 levels consistent with onset of cell death (Supplementary Fig. S1). In contrast, no reduction in C/EBPγ protein levels were

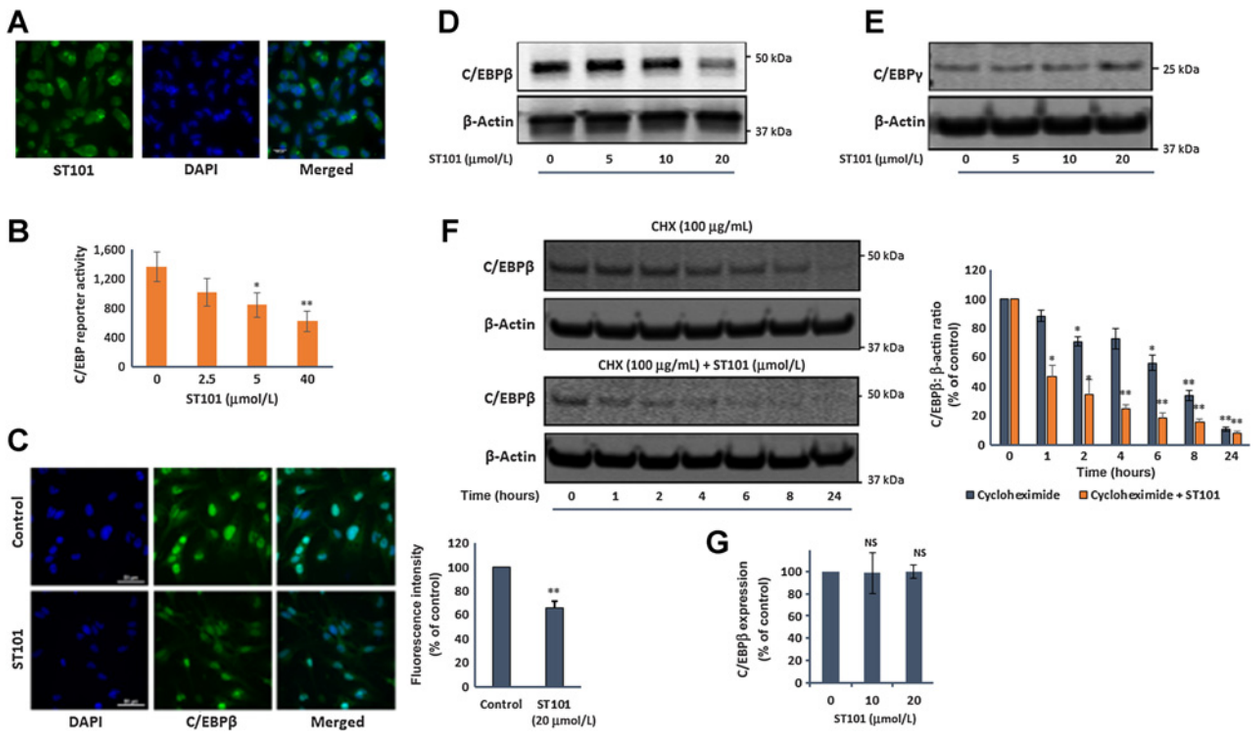

Figure 2.

ST101 enters cells and reduces C/EBPβ protein expression. **A,** Immunofluorescence detection of ST101 uptake into U251-LS cells exposed to 0.15 to 20 μmol/L peptide for 5 minutes. Representative images for cells exposed to 0.3 μmol/L ST101 are shown. **B,** Renilla luciferase gene was transiently expressed from a C/EBPβ responsive element in the presence and absence of ST101. ST101 induces a dose-dependent reduction in the expression of the luciferase gene (*, $P < 0.05$; **, $P < 0.01$). **C,** Immunofluorescence analysis of C/EBPβ expression in U251-LS cells treated ± 20 μmol/L ST101 for 24 hours. ImageJ was used for quantification of fluorescence intensity in each image. Each value is the mean ± SD of three images per condition (**, $P < 0.01$ vs. control). Scale bar represents 50 μm. **D,** Immunoblot of U251-LS total cell extracts treated with the indicated concentrations of ST101 for 24 hours, probed with antibodies against C/EBPβ and β-Actin. Note that the β-actin loading control in 2D is identical to that for **Fig. 5A**, as this membrane was stripped and re-probed to produce both figures. **E,** Immunoblot as in **D**, probed with antibodies against C/EBPγ and β-actin. **F,** Cycloheximide (CHX) chase analysis of C/EBPβ degradation in U251-LS cells. Representative western blots and graph of C/EBPβ protein levels after CHX (100 μg/mL) treatment ± 20 μmol/L ST101 in U251-LS cells. Results are the mean ± SD pooled from three independent experiments (*, $P < 0.05$; **, $P < 0.01$ vs. untreated control). C/EBPβ protein levels normalized to β-actin. **G,** Real-time RT-PCR of the transcript levels of C/EBPβ. Gene expression was normalized to β-actin (ns, not significant).

observed following treatment with ST101 in either cell line (**Fig. 2E**; Supplementary Fig. S6B), indicating that ST101 specifically targets C/EBPβ for degradation.

To investigate the impact of ST101 on the rate of C/EBPβ degradation, U251-LS cells were treated with 100 μg/mL cycloheximide to inhibit protein synthesis in the presence and absence of 20 μmol/L ST101. A significant reduction of 66 ± 4% ($P = 0.01$) in C/EBPβ protein level was observed after 8 hours of cycloheximide treatment in the absence of ST101 (**Fig. 2F**). Addition of ST101 accelerated C/EBPβ degradation in U251-LS cells, resulting in a 65 ± 10% reduction ($P = 0.04$) in C/EBPβ protein levels after 2 hours. The observed reduction in C/EBPβ protein expression was not due to transcriptional downregulation, as ST101 did not impact C/EBPβ transcript levels in U251-LS (**Fig. 2G**) or HCT116 (Supplementary Fig. S6C) cells exposed to 10 or 20 μmol/L ST101 for 24 hours.

ST101-induced proteasomal degradation of C/EBPβ is ubiquitin-dependent

To study the molecular mechanism of ST101-induced C/EBPβ downregulation, we investigated the impact of the proteasome inhibitor MG-132 on cells treated with 20 μmol/L ST101 for 24 hours.

ST101 for 24 hours. MG-132 increased baseline C/EBPβ expression (Supplementary Fig. S7A), consistent with published data (29). In cells exposed to ST101, MG-132 (2, 5, and 10 μmol/L) rescued C/EBPβ protein levels (U251-LS, HCT116, and A549 cell responses displayed in **Fig. 3A**, Supplementary Figs. S7B and S7C, respectively), indicating that ST101 targets C/EBPβ to the proteasome for degradation. The proteasome inhibitor Bortezomib (10, 50, and 100 nmol/L) similarly rescued ST101-induced C/EBPβ degradation in a concentration-dependent manner (**Fig. 3B**). To determine whether C/EBPβ degradation is mediated by ubiquitination, U251-LS cells were transiently transfected with myc-tagged C/EBPβ and exposed to ST101 for 24 hours. C/EBPβ ubiquitination was assessed by Western blot analysis following immunoprecipitation. As shown in **Fig. 3C**, a marked increase in myc-tagged C/EBPβ ubiquitination levels were observed after ST101 exposure. Similarly, Western blot analysis of endogenous C/EBPβ pulled down from lysates prepared from U251-LS cells 24 hours after ST101 treatment revealed a dose-dependent increase in ubiquitinated C/EBPβ compared with the untreated control (**Fig. 3D**). TAK-243, a small molecule inhibitor of ubiquitin-activating enzyme (UAE), reduced mono- and poly-ubiquitination of global cellular proteins in U251-LS cells in a concentration-dependent manner (Supplementary Fig. S7D), and similarly resulted in dose-dependent increase in C/EBPβ expression, suggesting that ubiquitination is required for ST101-induced C/EBPβ degradation (**Fig. 3E**). Densitometry of the impact of MG-132, Bortezomib, and TAK-243 on C/EBPβ expression after ST101 exposure are shown in **Fig. 3F**. Further, MLN4924-mediated inhibition of cullin-RING ligases (CRL), the largest class of ubiquitin E3 ligases (37), resulted in dose-dependent inhibition of C/EBPβ degradation (Supplementary Fig. S7E). Given the direct role of Peli1 E3 ubiquitin ligase in promoting degradation of C/EBPβ (38), we next investigated the impact of Peli1 knockdown on C/EBPβ expression post ST101 exposure. As shown in **Fig. 3G**, Peli1 knockdown, like MG132, increased C/EBPβ expression in control cells

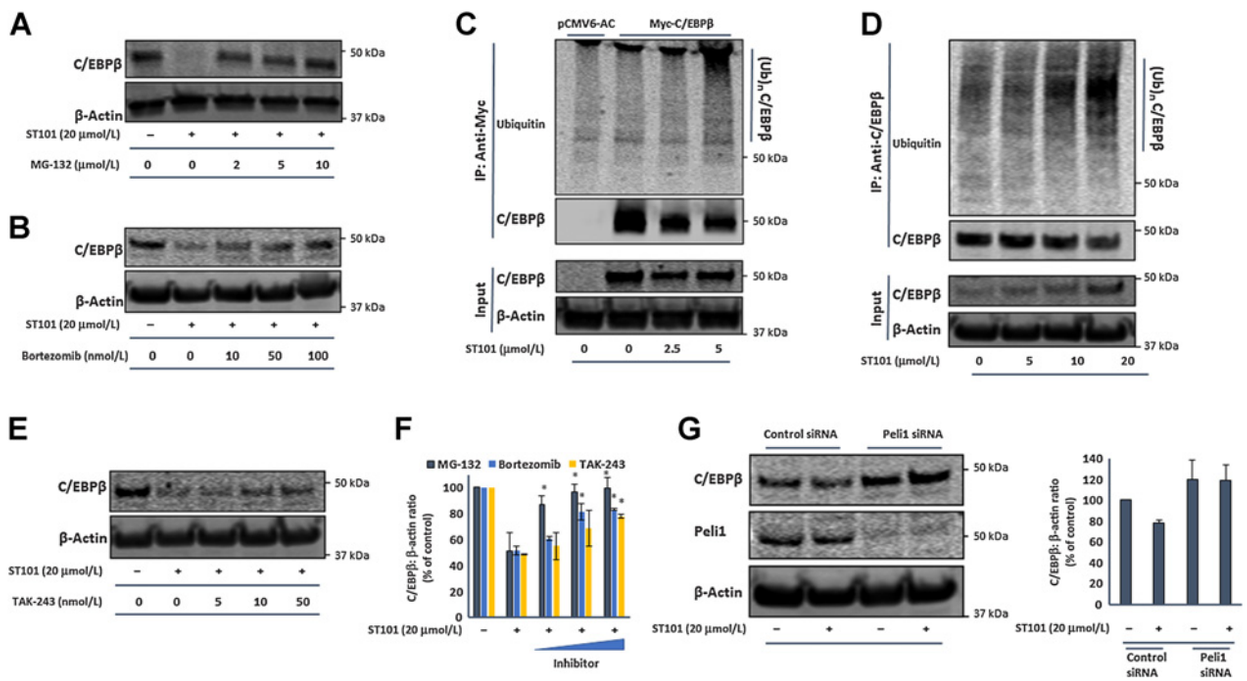

Figure 3.

ST101 targets C/EBPβ for ubiquitin-mediated proteasomal degradation. Immunoblot analysis of C/EBPβ protein level in U251-LS cells treated with ST101 (20 μmol/L) for 24 ± (**A**) MG-132 (2, 5, and 10 μmol/L) or (**B**) Bortezomib (10, 50, and 100 nmol/L). **C,** C/EBPβ ubiquitination post ST101 treatment in U251-LS cells transiently transfected with the indicated expression vectors following anti-Myc ip (top). Levels of input proteins in lysates without immunoprecipitation (below). **D,** Endogenous C/EBPβ ubiquitination post treatment with or without indicated concentrations of ST101 for 24 hours following i.p. pulldown of C/EBPβ (top). Levels of input proteins in lysates without immunoprecipitation (below). **E,** C/EBPβ protein levels in U251-LS cells treated with ST101 (20 μmol/L) for 24 ± TAK-243 (5, 10, and 50 nmol/L). **F,** Densitometry of results from **A**, **B**, and **E**. Graphs represent the ratio of total C/EBPβ to β-actin. **G,** Immunoblot and densitometry of C/EBPβ, Peli1, and β-actin (loading control) in control and Peli1-knockdown U251 cells ± 24 hours ST101 exposure (20 μmol/L).

and prevented ST101-induced C/EBPβ degradation, whereas control siRNA had no impact. Of note, 20 μmol/L ST101 resulted in 21 ± 3% reduction in C/EBPβ protein level in control siRNA treated cells, less than what is observed in nontransfected cells, likely a result of reduced ST101 cell penetration in the presence of positively charged liposomes used for transfection. Together, these data indicate that ST101-induced C/EBPβ degradation is mediated by the ubiquitin–proteasome pathway.

Transcriptomic analysis indicates ST101 impacts C/EBPβ target gene expression and signaling pathways

RNA-seq was performed on U251, A549, and MCF7 tumor cell lines after 24 hours ST101 exposure to assess the impact of C/EBPβ antagonism on global gene expression. Principal component (PC) analysis revealed consistency among biological replicates, as clusters of each cell line were observed with distinct pretreatment and posttreatment transcriptional profiles (**Fig. 4A**). ST101 resulted in 2,454, 1,443, and 116 differentially expressed transcripts ($P < 0.05$ and fold change ≥2) in U251, A549, and MCF7 cell lines, respectively (**Fig. 4B**). GSEA revealed that the gene sets most significantly enriched among the three contrasts were related to cell cycle and transcription factor networks (E2F, RUNX1, and MYC targets) that impact tumor cell survival and proliferation (**Fig. 4C**). In addition, downregulation of greater than 200 C/EBPβ target genes having at least one occurrence of the C/EBPβ binding site in regions spanning up to 4 kb around their transcription starting site was observed (**Fig. 4D**; Supplementary Table S6). The impact of ST101 on a select set of C/EBPβ target gene expression in U251, MCF7, and A549 cells by qPCR is shown in **Fig. 4E**. ST101 exposure (2.5–10 μmol/L) for 24 hours resulted in significant dose-dependent reductions in mRNA expression of prosurvival factors BCL2, BIRC3, and BIRC5, cell-cycle factors CCNB1 and CCNA2 and cyclin-dependent kinase CDK1 and ID family genes, ID1, ID2, and ID3 (**Fig. 4E**). A549 cells additionally displayed decreased mRNA expression of CCND3 and CDK2 (Supplementary Fig. S8).

Western blot analysis of U251-LS cells confirmed reductions in protein expression of C/EBPβ target genes (**Fig. 5A**), demonstrating that antagonism of C/EBPβ results in significant impact on gene expression of factors involved in cell survival, differentiation, and proliferation. The impact of MG-132 on C/EBPβ target gene expression was evaluated in U251-LS cells exposed to 20 μmol/L ST101 for 24 hours (**Fig. 5B**). MG-132 increased expression of ID1, ID3 and BIRC5 protein levels, indicating that ST101 impacts C/EBPβ target gene expression, at least in part, by enhancing C/EBPβ proteasomal degradation.

ST101 selectively induces cancer cell death

To evaluate whether ST101 impact on tumor cell gene expression is biologically relevant, assessment of ST101 on *in vitro* cell-cycle progression and cytotoxicity was performed. U251 and A549 cells were exposed to 1 and 5 μmol/L ST101 for 24 hours, and DNA content

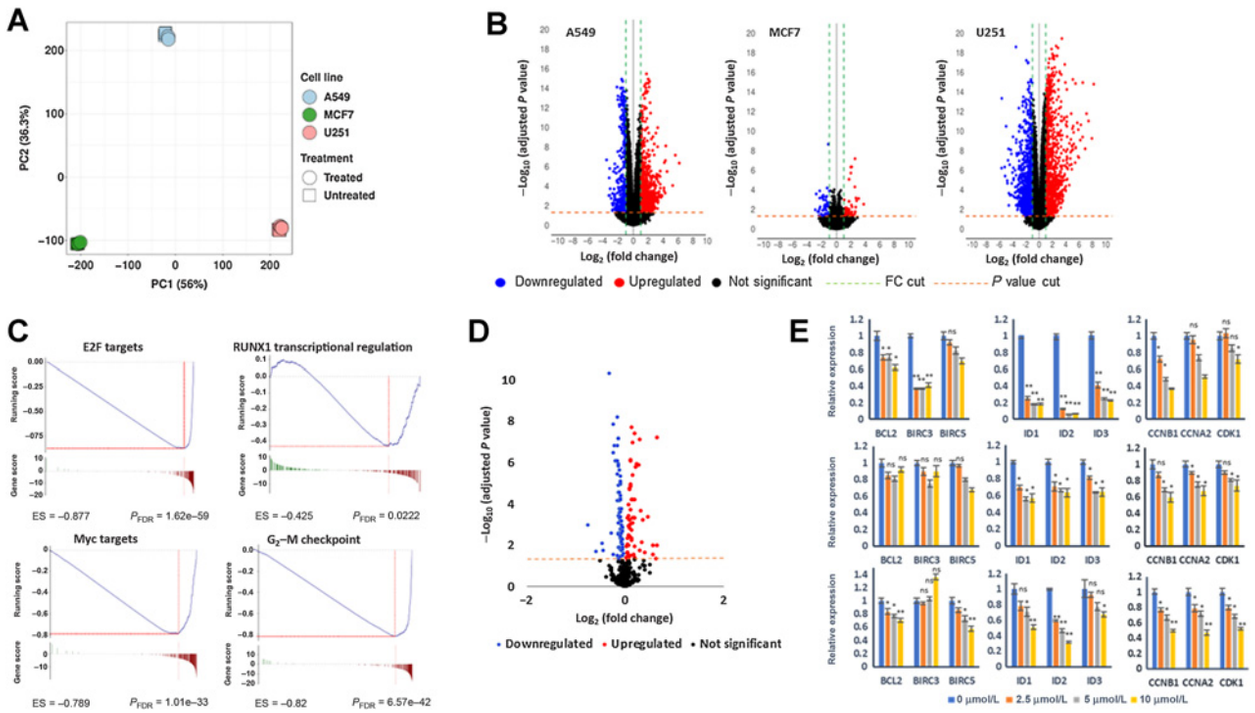

Figure 4.

ST101 modifies transcriptional profiles and subverts oncogenic pathways in cancer cells. **A,** Principal component (PC) analysis plot showing gene expression diversity across cell lines and treatment condition. **B,** Volcano plots showing the effect of ST101 on gene expression in A549, MCF7, and U251 cells. Significantly differentially expressed genes represented as red (upregulated) or blue (downregulated) dots. A representative subsample of nonsignificant genes (black) is displayed. Vertical green and horizontal red lines represent the fold change and *P* value thresholds applied, respectively. **C,** Functional GSEA analysis of DEGs in A549 demonstrates examples of pathways impacted by ST101. **D,** Volcano plots showing the effect of ST101 on CEBPβ target gene expression in A549 cells, analyzed as in **B**. **E,** qRT-PCR analysis of CEBPβ target genes after ST101 exposure in U251, MCF7, and A54 cells (2.5–10 μmol/L) compared with vehicle. Data represents log2 normalized expression ($2^{-\Delta\Delta Ct}$) and SEM. Error bars are means ± SD for assays performed in quadruplicate (*, $P < 0.05$; **, $P < 0.01$; ns, not significant as determined by Student *t* test).

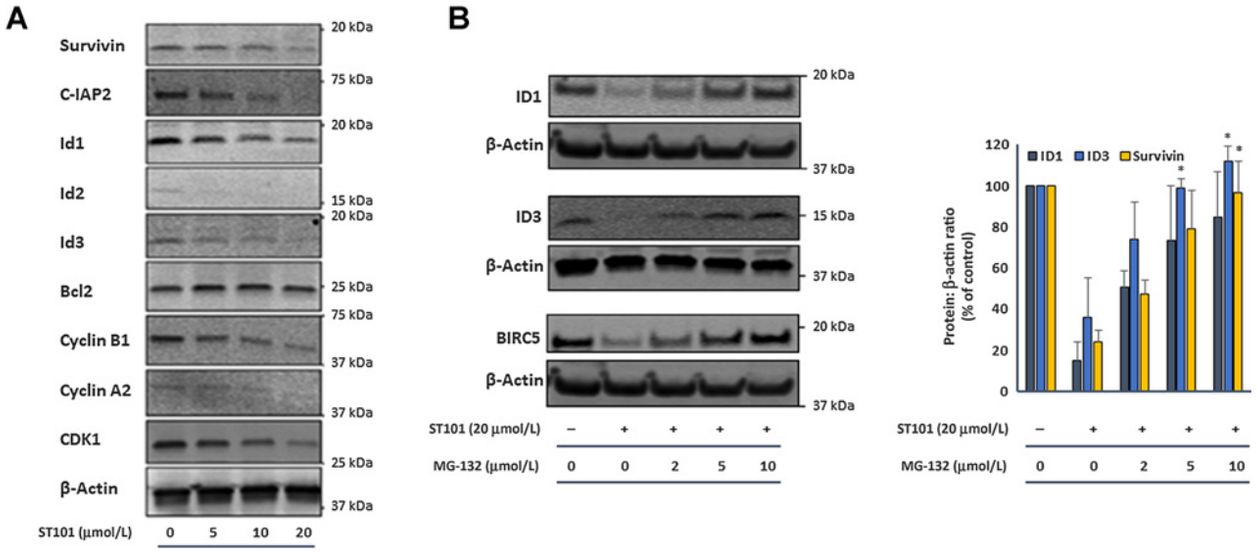

Figure 5.
Inhibition of the proteasome rescues C/EBPβ target gene expression after ST101 exposure. **A,** Immunoblot analysis of C/EBPβ target genes in U251 cells 24 hours after ST101 exposure (5–20 μmol/L ST101). Note that the β-actin loading control in **A** is identical to that for D, as the same membrane was stripped and reprobed to produce both figures. **B,** ID1, ID3, BIRC5, and β-actin expression in U251 cells following treatment with 20 μmol/L ST101 ± the indicated concentration of MG-132. Note that the β-actin loading controls for ID1 and BIRC5 are identical, as the same membrane was stripped and reprobed to produce both panels. Densitometric analysis was performed and total protein levels normalized to β-actin. Results represent the mean ± SD pooled from three independent experiments (*, $P < 0.05$; **, $P < 0.01$ vs. ST101 alone).

quantification and distribution was assessed by flow cytometry analysis following propidium iodide (PI) staining. ST101 exposure caused a dose-dependent increase in cells in G_1 phase, suggesting that ST101 causes cell-cycle arrest by blocking G_1 progression to S phase (**Fig. 6A** and **B**, respectively; representative histograms provided in Supplementary Fig. S9). After 24 hours exposure to 5 μmol/L ST101, the percentage of cells in G_1 increased in U251 cells from 35.1% to 57.8%, and in A549 cells increased from 54.5% to 75.3% ($P < 0.05$). These data suggest that ST101 induces cell-cycle arrest in cancer cells, indicating that ST101 possesses anti-proliferative activity.

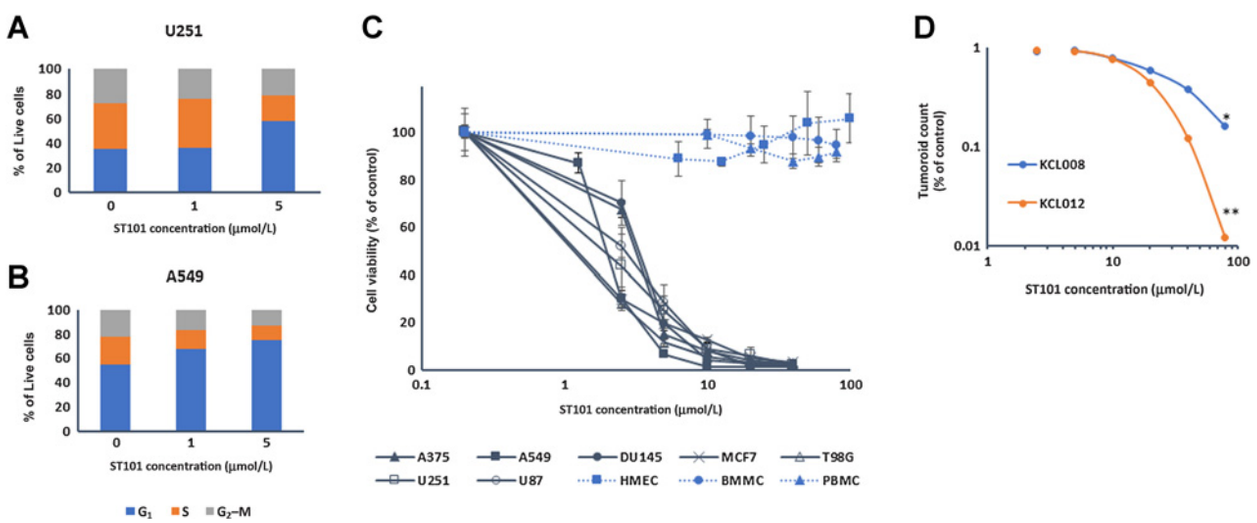

Figure 6.
ST101 inhibits proliferation and selectively induces cancer cell cytotoxicity. Cell-cycle analysis of (**A**) U251 and (**B**) A549 cells synchronized by thymidine block and exposed to ST101 for 24 hours. Data represents the percentage of cells displaying representative staining of G_1, S, or G_2–M phase from one of three representative experiments, $n = 3$/experiment. **C,** Cell viability of A375, A549, DU145, LNCap, MCF7, T98G, U251, and U87 tumor cell lines exposed to 2.5 to 40 μmol/L ST101, HMEC exposed to 2.5 to 100 μmol/L ST101, and human peripheral blood and bone marrow-derived mononuclear cells exposed to 1.25 to 80 μmol/L ST101 for 48 hours. Viability is presented as percent of vehicle-treated control. Data represents mean ± SEM for a minimum of three replicates from three independent experiments for each data point [*, $P < 0.05$; **, $P < 0.01$ vs. control, unpaired *t* test, and multiple-comparison correction using Bonferroni–Dunn correction ($\alpha = 0.01$)]. **D,** Patient-derived breast cancer tumoroid viability following 7-day exposure to ST101 (0–100 μmol/L). Each data point represents mean ± SEM for four replicates.

The impact of ST101 on tumor cell death was evaluated across a panel of cell lines. High-content imaging indicated near complete cytotoxic activity at concentrations equal to or exceeding 10 μmol/L in sensitive cell lines, as indicated by greater than 95% of cells staining annexin V^{high} and PI^{high}. A mean EC_{50} value of 2.1 ± 0.4 μmol/L was observed following 48 hours exposure (**Fig. 6C**). In contrast, flow cytometric analysis indicated that normal PBMCs and BMMCs are not sensitive to ST101 and did not reach an EC_{50} value at 80 μmol/L, the highest concentration of ST101 tested (**Fig. 6C**). Similarly, normal human mammary epithelial cells (HMEC) did not reach an EC_{50} value at 100 μmol/L, the highest concentration of ST101 tested (**Fig. 6C**). These data indicate that ST101 exerts selective cytolytic activity against tumor cell lines compared with normal cells. Evaluation in patient-derived breast cancer organoids indicated ST101 exposure resulted in a dose-dependent reduction in proliferation and viability (**Fig. 6D**). Tumor organoids grown in 3-dimensional culture demonstrated EC_{50} values of 18.56 and 15.32 μmol/L, respectively, in KCL008 ($Her2^+$/ER^-/PR^-) and KCL012 ($Her2^-$/ER^-/PR^-) breast cancer cells.

ST101 displays broad antitumor activity *in vivo*

Initial *in vivo* studies evaluated the pharmacokinetic parameters of ST101 following a single 25 mg/kg intravenous or subcutaneous ST101 injection. IV dosing resulted in a C_{max} value of 27,100 ng/mL and an AUC_{last} of 16,400 hr*ng/mL. Bioavailability following SC dosing was approximately 66%, resulting in a C_{max} of 1,750 ng/mL and an observed AUC_{last} of 10,900 hr*ng/mL (**Fig. 7A**). Calculated plasma half-life of ST101 after IV and SC dosing was 12.8 and 8.3 hrs, respectively.

Administration of ST101 to mice bearing U251 GBM subcutaneous xenograft resulted in potent tumor growth inhibition (%ΔTGI). Tumor-bearing NOD scid mice (average tumor volume of 220 mm^3) treated with 50 mg/kg ST101 three times per week for three weeks by subcutaneous (SC) injection resulted in durable tumor regressions and a 97.1% tumor growth inhibition (**Fig. 7B**; $P < 0.0001$ vs. control). Gross evaluation at the end of the 90-day study indicated that 50% (3/6) of treated animals were tumor-free. No impact of ST101 on body weight was observed (Supplementary Fig. S10A). Quantitative PCR analysis of U251 tumor samples (mean volume of 180 mm^3) collected from mice 6 hours after treatment with ST101 (25 mg/kg once (QDx1) or three consecutive days (QDx3) indicated a significant decrease in BIRC3 and ID2 expression compared to vehicle treated control tumors (72.1% and 26.3% decreased ID2 and BIRC3 expression, respectively; **Fig. 7C**; $P < 0.05$ for each vs. control).

Following surgical resection, the DNA methylating agent temozolomide (TMZ) along with radiotherapy is standard of care for newly diagnosed GBM, with a clinically meaningful survival benefit compared to radiotherapy alone, however 2-year survival remains less than 20% (39). As C/EBPβ expression has been implicated in resistance of GBM to TMZ by impacting cell cycle and DNA replication (40), and

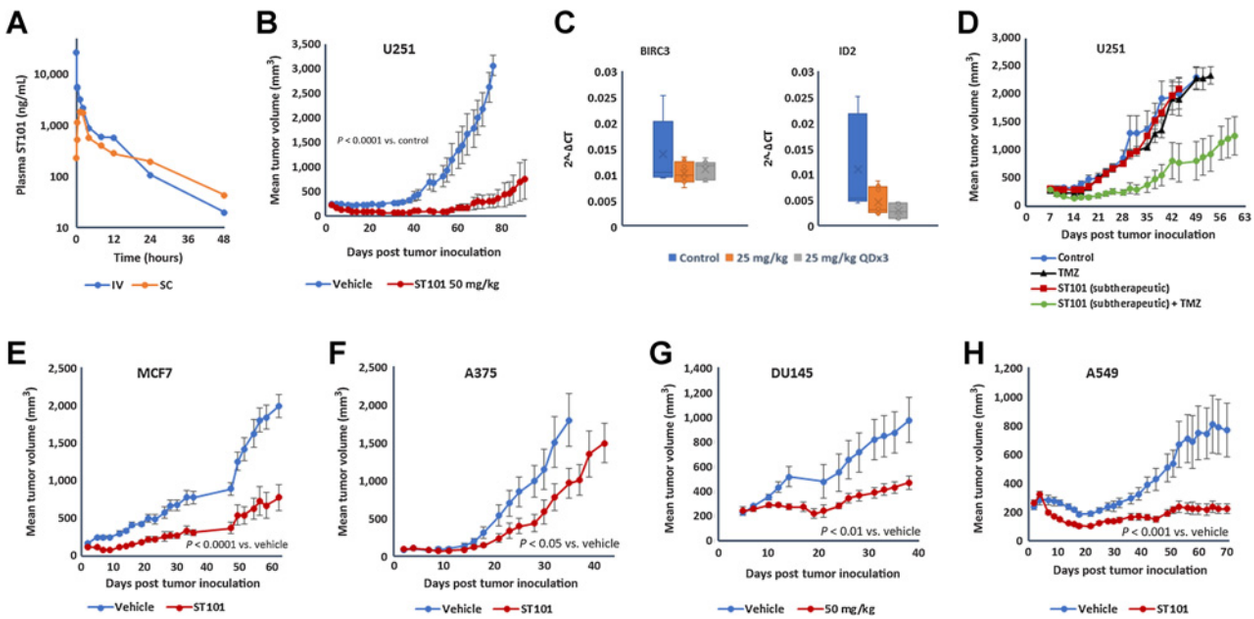

Figure 7.

ST101 displays potent anti-tumor activity in mouse subcutaneous xenograft models. **A,** Plasma concentration of ST101 in C57BL/6 mice at the indicated times following 25 mg/kg SC or IV injection. **B,** ST101 administration (50 mg/kg administered three days per week for three weeks by SC injection) to mice bearing U251 glioblastoma xenografts was initiated on tumors with an average volume of 220 mm^3. Wilcoxon matched-pairs signed rank test indicated significant difference in tumor growth between ST101 and vehicle ($P < 0.0001$; $n = 7$ mice/group). **C,** qPCR analysis of U251 tumors collected and processed 6 hours following 1 or 3 consecutive days administration of 25 mg/kg ST101 on day 14. **D,** U251 tumors were grown as in **A**, and subtherapeutic ST101 (10 mg/kg administered 3 days per week for 3 weeks), temozolomide (100 mg/kg administered 3 days per week for 1 week by oral gavage) or combination of ST101 and temozolomide were administered. $P < 0.001$ for combination group vs. vehicle or single-agents; $n = 5$–6 mice/group. **E,** Nude mice bearing MCF7 xenografts were administered ST101 (25 mg/kg three times per week for 3 weeks) starting on day 2 posttumor inoculation ($P < 0.001$ for ST101 vs. vehicle; $n = 8$ mice in vehicle and $n = 4$ mice in ST101 group). **F,** Nude mice bearing A375 melanoma xenografts were administered ST101 (25 mg/kg 5 days per week for 3 weeks) starting on day 2 posttumor implant ($P < 0.05$ for ST101 vs. vehicle; $n = 6$–7 mice/group). **G,** Nude mice receiving DU145 prostate cancer xenografts were administered ST101 (50 mg/kg 3 days per week for 3 weeks starting on day 7 posttumor inoculation; $P < 0.01$ for ST101 vs. vehicle; $n = 6$ mice/group). **H,** Nude mice receiving A549 lung adenocarcinoma xenografts were administered ST101 (25 mg/kg 5 days per week for 3 weeks) starting on day 2 posttumor inoculation ($P < 0.001$ for ST101 vs. vehicle; $n = 8$ mice/group).

ST101 is shown to impact gene expression profiles that impact these pathways (**Fig. 4**), ST101 was evaluated in combination with TMZ in GBM subcutaneous xenograft models. In the U251 model, a subtherapeutic dose of 10 mg/kg ST101 administered three times per week for three weeks in combination with 100 mg/kg TMZ administered orally three times per week for 1 week (**Fig. 7D**) resulted in 74.6% TGI on day 49 ($P < 0.001$ for ST101 + TMZ combination vs. either single agent or control). Neither subtherapeutic ST101 nor TMZ alone significantly impacted tumor growth compared to control animals. No impact of ST101 on body weight was observed (Supplementary Fig. S10B). Similar results were observed in a T98G (O^6-methylguanine methyltransferase $(MGMT)^+/p53^+$) xenograft model (Supplementary Fig. S11). To support potential development of ST101 for glioblastoma, immunohistochemistry studies were performed on brain sections from naïve C57BL/6 mice two hours following IV administration of ST101. Data indicates uptake in microvasculature and glial cells, demonstrating ST101 penetration past an intact blood brain barrier in mice (Supplementary Fig. S12). These data indicate that ST101 displays anti-GBM activity both as a single agent and in combination with TMZ.

ST101 antitumor activity was similarly evaluated in subcutaneous xenograft models of MCF7 breast adenocarcinoma, A375 melanoma, DU145 prostate cancer, and A549 lung adenocarcinoma. MCF7 xenograft tumors treated with 25 mg/kg ST101 three times per week for 3 weeks resulted in 61.8% TGI (**Fig. 7E**, $P < 0.001$ for ST101 vs. control tumors). A375 melanoma tumor fragment xenografts treated with 25 mg/kg ST101 five times per week, resulting in 46.3% TGI on day 35 posttumor inoculation (**Fig. 7F**, $P < 0.05$ for ST101 vs. control tumors). DU145 xenograft tumors treated with 50 mg/kg ST101 three times per week by SC injection resulted in 69.5% TGI (**Fig. 7G**, $P < 0.01$ for ST101 vs. vehicle control-treated tumors), and A549 lung carcinoma xenografts treated with 25 mg/kg ST101 five times per week resulted in durable and sustained tumor regression throughout the 70-day study (**Fig. 7H**, $P < 0.001$ for ST101 vs. vehicle control-treated tumors). These data indicate that ST101 displays antitumor activity across a panel of diverse xenograft models. In all studies, no significant impact on body weight was observed (Supplementary Figs. S10C–S10F). As human and mouse C/EBPβ leucine zipper domain have 100% homology, lack of weight loss in mice suggests that ST101 does not induce on-target toxicity. Further, ELISA detection of anti-ST101 antibodies indicate that ST101 is non-immunogenic. In C57BL/6 mice immunized once weekly with 10 mg/kg ST101 by intravenous injection, no ST101-specific antibody titer was observed (Supplementary Fig. S13).

Discussion

C/EBPβ is an emerging and attractive target that contributes to tumor cell survival and proliferation. Aberrant expression is reported in several epithelial tumors such as glioblastoma, where patients with highest C/EBPβ expression are associated with worse outcomes ($P = 0.011$; ref. 14). Various reports indicate that C/EBPβ expression is prognostic of clinical responses in breast cancer ($P = 0.005$; refs. 10, 23), prostate cancer ($P < 0.001$; ref. 22), ovarian cancer ($P = 0.0099$), and renal cell carcinoma ($P < 2.4e{-}12$; ref. 17). Here, we describe the C/EBPβ antagonist, ST101, which inhibits C/EBPβ DNA binding and results in targeted C/EBPβ proteasomal degradation. ST101 displays robust *in vitro* and *in vivo* antitumor activity in multiple human xenograft tumor models.

Self-association to form dimers and higher-order oligomers is a common property of proteins and represents a recurring theme in biological systems. Several structural and biophysical studies show that protein dimerization is a key factor in the regulation of enzymes, ion channels, receptors, and transcription factors (41). Transcription factors containing bZIP, basic helix-loop-helix (bHLH), MADS box, or Rel homology domains require noncovalent dimerization to bring adjacent basic regions that bind DNA together to confer specificity. Once the dimer is lost, these transcription factors lose the ability to recognize and bind specific sequences of nucleic acids (41, 42). ST101 was designed based on this premise. Our initial experiments indicate that ST101 disruption of C/EBPβ dimerization impacts C/EBPβ DNA binding. Analytical data confirmed that ST101 disrupts C/EBPβ dimerization and inhibited its activity, as measured by DNA-binding ELISA. Subsequent RNA-seq analysis confirmed that ST101 significantly impacts gene expression in epithelial tumor cells. GSEA of these datasets revealed that ST101 exposure impacted genes involved in cell cycle, transcription factor networks, cell death pathways, and cancer signaling networks, suggesting the potential of ST101 as a targeted therapeutic for C/EBPβ-driven cancers.

In addition to functionality, dimerization has a fundamental role in protein stabilization. Monod and colleagues demonstrated that homodimeric protein associations result in closed structures, with an intrinsic symmetry and enhanced stability (43). Self-association of nitric oxide synthase provides an example of homodimerization preventing ubiquitin−proteasomal degradation (44). Similarly, C/EBP family transcription factors evade ubiquitin–proteasome-mediated degradation by forming dimers via leucine zipper domain interactions. Deletion of the C/EBPβ leucine zipper domain has been shown to prevent dimerization and enhance degradation (29), suggesting that the proteasome represents a mechanism for regulating the basal level of intracellular C/EBP proteins. Our experiments investigating ST101 impact on C/EBPβ stability revealed that ST101 accelerated C/EBPβ degradation via a ubiquitin-dependent process. Cycloheximide chase experiments indicate that whereas C/EBPβ protein expression is reduced by greater than 50% after 8 hours in cells where protein synthesis is inhibited, a similar loss of C/EBPβ protein expression is observed after 1 hour in cells exposed to ST101, and degradation could be attenuated by inhibition of the proteasome. Despite structural similarity between C/EBP family members, ST101 binding to C/EBPβ appears to be exquisitely specific, as the measured ST101 K_D for C/EBPβ is approximately 3,000-fold lower than that for C/EBPγ. Furthermore, ST101 does not result in proteasomal degradation of C/EBPγ at biologically relevant levels. Thus, antagonists of transcription factor dimerization present a unique opportunity to specifically degrade previously undruggable targets such as C/EBPβ.

Targeted protein degradation is an alternative to conventional chemotherapeutics and small molecule-based targeted therapeutics. Proteolysis-targeting chimera (PROTAC) is a prominent approach, where a ligand (mostly small-molecule inhibitors) of the protein of interest is covalently linked to a ligand of an E3 ubiquitin ligase. Advantages of targeted protein degradation over conventional drugs include the ability to impact targets harboring mutations leading to its overexpression, which result in decreased small molecule binding, or that introduce bypass resistance mechanisms (45). ST101 offers the unique therapeutic opportunity to induce targeted degradation of C/EBPβ as well as specifically antagonize its interaction with DNA, suggesting activity even in the absence of the proteasome. Further, as C/EBPβ expression decreases, local ST101 concentration remains relatively unchanged due to its resistance to proteolytic degradation.

Thus, we hypothesize that the ratio of ST101 to C/EBPβ increases over time, increasing the rate of ST101 binding to remaining C/EBPβ, further enhancing C/EBPβ degradation and allowing for potent ST101 activity even at low concentrations.

Functionally, ST101 displays potent and selective antitumor activity *in vitro* and *in vivo*. ST101 induced dose-dependent cell death across a panel of tumor cell lines in standard 2-dimensional culture conditions, with a mean EC_{50} value of 2.1 ± 0.43 μmol/L. In contrast, ST101 did not significantly impact viability of normal HMECs or PBMCs, demonstrating tumor cell-specific cytotoxicity. Similar observations were reported in a Ras-driven skin tumor model, where genetic inactivation of C/EBPβ resulted in synthetic lethality of tumor cells, whereas normal neighboring cells were not impacted (46). These data suggest that non-tumor cells that do not rely on C/EBPβ-mediated signals for proliferation and survival are not sensitive to ST101. Supporting this hypothesis, repeat-dose administration of ST101 resulted in significant antitumor activity *in vivo* without impacting body weight or inducing organ toxicity.

With cures remaining scarce in patients with advanced solid tumors, there is an unmet medical need for more effective and less toxic therapies. This study provides the First Disclosure of ST101, an antagonist of the oncogenic transcription factor C/EBPβ with significant and selective antitumor activity. Data presented herein validate C/EBPβ as a bona fide drug target for cancer therapy and demonstrate that targeted antagonism of C/EBPβ with a cell-penetrating peptide represents a powerful strategy with potential to broadly impact patients with advanced solid tumors. These data also provide proof-of-concept support for cell-penetrating peptide approaches to target previously "undruggable" cancer targets. Based on its significant preclinical activity, ST101 has advanced into a Phase I/II clinical study designed to determine the safety, tolerability, PK, PD, and proof-of-concept efficacy of ST101 in patients with advanced unresectable and metastatic solid tumors.

Authors' Disclosures

L. Ghamsari reports grants from NIH during the conduct of the study. S.F. Leong reports grants from NIH during the conduct of the study. R. Ramirez reports grants from NIH during the conduct of the study. M. Koester reports grants from NIH during the conduct of the study. E. Gallagher reports grants from NIH during the conduct of the study. G. Merutka reports grants from NIH during the conduct of the study; also has a patent 10,525,100 issued to Sapience Therapeutics. B.J. Kappel reports a patent 10,525,100 issued. J.A. Rotolo reports grants from NIH during the conduct of the study; also has a patent for US Patent No. 10,525,100 issued. No disclosures were reported by the other authors.

Authors' Contributions

E. Darvishi: Data curation, formal analysis, investigation, writing–original draft. **L. Ghamsari:** Formal analysis, investigation, writing–review and editing. **S.F. Leong:** Data curation. **R. Ramirez:** Formal analysis. **M. Koester:** Data curation. **E. Gallagher:** Investigation. **M. Yu:** Data curation, investigation. **J.M. Mason:** Conceptualization, resources, data curation, formal analysis, supervision. **G. Merutka:** Conceptualization, writing–review and editing. **B.J. Kappel:** Conceptualization, formal analysis, writing–review and editing. **J.A. Rotolo:** Conceptualization, formal analysis, supervision, writing–review and editing.

Acknowledgments

Part of this work was supported by NIH grant R43CA250786. We thank New York Medical College Department of Comparative Medicine and Hong Zhao of the Department of Molecular Cytology for their contributions. We thank Fios Genomics for bioinformatics analysis of RNA-seq data sets and figure generation. We thank Dr. Gina Capiaux and Dr. Alice Bexon for critical and technical review of the manuscript.

Note

Supplementary data for this article are available at Molecular Cancer Therapeutics Online (http://mct.aacrjournals.org/).

Received November 30, 2021; revised April 29, 2022; accepted September 14, 2022; published first September 16, 2022.

References

1. Zahnow CA. CCAAT/enhancer binding proteins in normal mammary development and breast cancer. Breast Cancer Res 2002;4:113–21.
2. Westmacott A, Burke ZD, Oliver G, Slack JM., Tosh D. C/EBPalpha and C/EBPbeta are markers of early liver development. Int J Dev Biol 2006;50:653–7.
3. Hirata M, Kugimiya F, Fukai A, Ohba S, Kawamura N, Ogasawara T, et al. C/EBPbeta Promotes transition from proliferation to hypertrophic differentiation of chondrocytes through transactivation of p57. PLoS One 2009;4:e4543.
4. Hattori T, Ohoka N, Hayashi H, Onozaki K. C/EBP homologous protein (CHOP) up-regulates IL-6 transcription by trapping negative regulating NF-IL6 isoform. FEBS Lett 2003;541:33–9.
5. Lee LL, Kim SJ, Hahn YI, Jang JH, Saeidi S, Surh YJ. Stabilization of C/EBPbeta through direct interaction with STAT3 in H-Ras transformed human mammary epithelial cells. Biochem Biophys Res Commun 2021;546:130–7.
6. Poli V. The role of C/EBP isoforms in the control of inflammatory and native immunity functions. J Biol Chem 1998;273:29279–82.
7. Screpanti I, Romani L, Musiani P, Modesti A, Fattori E, Lazzaro D, et al. Lymphoproliferative disorder and imbalanced T-helper response in C/EBP beta-deficient mice. EMBO J 1995;14:1932–41.
8. Tanaka T, Akira S, Yoshida K, Umemoto M, Yoneda Y, Shirafuji N, et al. Targeted disruption of the NF-IL6 gene discloses its essential role in bacteria killing and tumor cytotoxicity by macrophages. Cell 1995;80:353–61.
9. Lekstrom-Himes J, Xanthopoulos KG. Biological role of the CCAAT/enhancer-binding protein family of transcription factors. J Biol Chem 1998;273:28545–8.
10. Zahnow CA. CCAAT/enhancer-binding protein beta: its role in breast cancer and associations with receptor tyrosine kinases. Expert Rev Mol Med 2009;11:e12.
11. Piwien-Pilipuk G, MacDougald O, Schwartz J. Dual regulation of phosphorylation and dephosphorylation of C/EBPbeta modulate its transcriptional activation and DNA binding in response to growth hormone. J Biol Chem 2002;277:44557–65.
12. Aguilar-Morante D, Cortes-Canteli M, Sanz-Sancristobal M, Santos A, Perez-Castillo A. Decreased CCAAT/enhancer binding protein beta expression inhibits the growth of glioblastoma cells. Neuroscience 2011;176:110–9.
13. Gardiner JD, Abegglen LM, Huang X, Carter BE, Schackmann EA, Stucki M, et al. C/EBPbeta-1 promotes transformation and chemoresistance in Ewing sarcoma cells. Oncotarget 2017;8:26013–26.
14. Homma J, Yamanaka R, Yajima N, Tsuchiya N, Genkai N, Sano M, et al. Increased expression of CCAAT/enhancer binding protein beta correlates with prognosis in glioma patients. Oncol Rep 2006;15:595–601.
15. Kim MH, Fields J. Translationally regulated C/EBP beta isoform expression upregulates metastatic genes in hormone-independent prostate cancer cells. Prostate 2008;68:1362–71.
16. Li W, Kessler P, Yeger H, Alami J, Reeve AE, Heathcott R, et al. A gene expression signature for relapse of primary wilms tumors. Cancer Res 2005;65:2592–601.
17. Oya M, Horiguchi A, Mizuno R, Marumo K, Murai M. Increased activation of CCAAT/enhancer binding protein-beta correlates with the invasiveness of renal cell carcinoma. Clin Cancer Res 2003;9:1021–7.

18. Pal R, Janz M, Galson DL, Gries M, Li S, Johrens K, et al. C/EBPbeta regulates transcription factors critical for proliferation and survival of multiple myeloma cells. Blood 2009;114:3890–8.
19. Rask K, Thorn M, Ponten F, Kraaz W, Sundfeldt K, Hedin L, et al. Increased expression of the transcription factors CCAAT-enhancer binding protein-beta (C/EBBeta) and C/EBzeta (CHOP) correlate with invasiveness of human colorectal cancer. Int J Cancer 2000;86:337–43.
20. Heckman CA, Wheeler MA, Boxer LM. Regulation of Bcl-2 expression by C/EBP in t(14;18) lymphoma cells. Oncogene 2003;22:7891–9.
21. Sundfeldt K, Ivarsson K, Carlsson M, Enerback S, Janson PO, Brannstrom M, et al. The expression of CCAAT/enhancer binding protein (C/EBP) in the human ovary in vivo: specific increase in C/EBPbeta during epithelial tumour progression. Br J Cancer 1999;79:1240–8.
22. Adamo H, Hammarsten P, Hagglof C, Dahl Scherdin T, Egevad L, Stattin P, et al. Prostate cancer induces C/EBPbeta expression in surrounding epithelial cells which relates to tumor aggressiveness and patient outcome. Prostate 2019;79:435–45.
23. van de Vijver MJ, He YD, van't Veer LJ, Dai H, Hart AA, Voskuil DW, et al. A gene-expression signature as a predictor of survival in breast cancer. N Engl J Med 2002;347:1999–2009.
24. Bushweller JH. Targeting transcription factors in cancer - from undruggable to reality. Nat Rev Cancer 2019;19:611–24.
25. Yan C, Higgins PJ. Drugging the undruggable: transcription therapy for cancer. Biochim Biophys Acta 2013;1835:76–85.
26. Ramji DP, Foka P. CCAAT/enhancer-binding proteins: structure, function and regulation. Biochem J 2002;365:561–75.
27. Asada R, Kanemoto S, Kondo S, Saito A, Imaizumi K. The signalling from endoplasmic reticulum-resident bZIP transcription factors involved in diverse cellular physiology. J Biochem 2011;149:507–18.
28. Potapov V, Kaplan JB, Keating AE. Data-driven prediction and design of bZIP coiled-coil interactions. PLoS Comput Biol 2015;11:e1004046.
29. Hattori T, Ohoka N, Inoue Y, Hayashi H, Onozaki K. C/EBP family transcription factors are degraded by the proteasome but stabilized by forming dimer. Oncogene 2003;22:1273–80.
30. Fields GB, Noble RL. Solid phase peptide synthesis utilizing 9-fluorenylmethoxycarbonyl amino acids. Int J Pept Protein Res 1990;35:161–214.
31. Mason JM, Hagemann UB, Arndt KM. Improved stability of the Jun-Fos Activator Protein-1 coiled coil motif: A stopped-flow circular dichroism kinetic analysis. J Biol Chem 2007;282:23015–24.
32. Livak KJ, Schmittgen TD. Analysis of relative gene expression data using real-time quantitative PCR and the 2(-Delta Delta C(T)) Method. Methods 2001;25:402–8.
33. Thoren PE, Persson D, Karlsson M, Norden B. The antennapedia peptide penetratin translocates across lipid bilayers—the first direct observation. FEBS Lett 2000;482:265–8.
34. Waizenegger T, Fischer R, Brock R. Intracellular concentration measurements in adherent cells: a comparison of import efficiencies of cell-permeable peptides. Biol Chem 2002;383:291–9.
35. Becktel WJ, Schellman JA. Protein stability curves. Biopolymers 1987;26:1859–77.
36. Vinson CR, Sigler PB, McKnight SL. Scissors-grip model for DNA recognition by a family of leucine zipper proteins. Science 1989;246:911–6.
37. Soucy TA, Smith PG, Milhollen MA, Berger AJ, Gavin JM, Adhikari S, et al. An inhibitor of NEDD8-activating enzyme as a new approach to treat cancer. Nature 2009;458:732–6.
38. Xu J, Yu T. Peli1 impairs microglial Aβ phagocytosis through promoting C/EBPβ degradation. PLoS Biol 2020;18:e3000837.
39. van Genugten JA, Leffers P, Baumert BG, Tjon AFH, Twijnstra A. Effectiveness of temozolomide for primary glioblastoma multiforme in routine clinical practice. J Neurooncol 2010;96:249–57.
40. Gao Y, Liu B, Feng L, Sun B, He S, Yang Y, et al. Targeting JUN, CEBPB, and HDAC3: a novel strategy to overcome drug resistance in hypoxic glioblastoma. Front Oncol 2019;9:33.
41. Marianayagam NJ, Sunde M, Matthews JM. The power of two: protein dimerization in biology. Trends Biochem Sci 2004;29:618–25.
42. Funnell AP, Crossley M. Homo- and heterodimerization in transcriptional regulation. Adv Exp Med Biol 2012;747:105–21.
43. Monod J, Wyman J, Changeux JP. On the nature of allosteric transitions: a plausible model. J Mol Biol 1965;12:88–118.
44. Dunbar AY, Kamada Y, Jenkins GJ, Lowe ER, Billecke SS, Osawa Y. Ubiquitination and degradation of neuronal nitric-oxide synthase *in vitro*: dimer stabilization protects the enzyme from proteolysis. Mol Pharmacol 2004;66:964–9.
45. Li X, Song Y. Proteolysis-targeting chimera (PROTAC) for targeted protein degradation and cancer therapy. J Hematol Oncol 2020;13:50.
46. Messenger ZJ, Hall JR, Jima DD, House JS, Tam HW, Tokarz DA, et al. C/EBPbeta deletion in oncogenic Ras skin tumors is a synthetic lethal event. Cell Death Dis 2018;9:1054.